

## Modeling the interface area aspect ratio of carbide grains in WC–Co composites



Xiaokun Yuan<sup>a,\*</sup>, Gregory S. Rohrer<sup>b</sup>, Xiaoyan Song<sup>a</sup>, Harry Chien<sup>b</sup>, Jia Li<sup>b</sup>

<sup>a</sup> College of Materials Science and Engineering, Beijing University of Technology, Beijing 100124, China

<sup>b</sup> Department of Materials Science and Engineering, Carnegie Mellon University, Pittsburgh, PA 15213-3890, USA

### ARTICLE INFO

#### Article history:

Received 7 November 2013

Accepted 11 January 2014

Available online 23 January 2014

#### Keywords:

Cemented carbide

Electron backscattered diffraction

Interface area aspect ratio

Five parameter analysis

### ABSTRACT

The average interface area aspect ratios of carbide grains in WC–Co composites are measured from basal-to-prismatic area ratios determined by the five parameter analysis (FPA) method. Grain boundary plane distributions regardless of misorientations indicate that the (0001) basal and  $(10\bar{1}0)$  prismatic planes are the most common habit planes, and the interface area aspect ratio is determined by the ratio of the (0001) plane area to the  $(10\bar{1}0)$  plane area. Additionally, the measured aspect ratios are found to vary with the densification mechanisms of the WC–Co composites. The work offers a new alternative to characterize the geometry of carbide grains in WC–Co composites.

© 2014 Elsevier Ltd. All rights reserved.

### 1. Introduction

WC–Co composites have outstanding mechanical properties and are widely used in industrial applications. The mechanical properties of WC–Co composites are strongly influenced by their microstructures, which can be described as carbide grains embedded in cobalt. Such dense polycrystalline materials consist of irregularly shaped, approximately polygonal, single carbide crystals joined at internal interfaces referred to as grain boundaries [1]. Many studies have shown that the geometry of the carbide grains can affect the mechanical properties of WC–Co composites [2,3]. For example, the formation of plate-like carbide crystals can increase the fracture toughness of WC–Co composites [2], and the fracture strength of tungsten carbide decreases as the length along the c-axis increases [3].

The aspect ratio is an important parameter to characterize the geometry of carbide grains. Using the conventional definition from two-dimensional studies [4], the aspect ratio is defined as the length of the longest axis divided by the length of the shortest axis of a certain grain, without consideration of the crystal orientation. In other work, the aspect ratio [5] is defined as the length of the minor axis divided by the length of the major axis of the ellipse that fits to the grain perimeter according to the least squares method. In addition, other aspect ratio definitions have accounted for the three-dimensional shape of the crystal. For example, in reference [6], two kinds of aspect ratios are used to describe the carbide grain shape: one is the ratio between the lengths of the short and long

prismatic facets (assuming six sided trigonal prisms), and the other is the ratio between the thickness along the  $\langle 0001 \rangle$  direction and the width of the basal plane. In reference [7], the aspect ratio is defined as the ratio between the thickness along the  $\langle 0001 \rangle$  direction and the length of the basal facet. These definitions present various descriptions about the geometry of carbide grains; nevertheless, using these definitions, each grain should be counted separately to obtain its aspect ratio value, and the statistical description about the geometry can merely be realized through the cumulated frequency of aspect ratios [7].

There exist methods to determine the preferred orientation of crystallites in the structure of polycrystalline materials, and moreover, it has recently been demonstrated that the average three-dimensional crystal habits can be determined by combining the geometric information found in conventional micrographs with crystal orientation data [8]. This approach has been extended to the so-called “five parameter analysis (FPA)” method that uses stereology to estimate the relative areas of grain boundary planes as a function of lattice misorientation (three parameters) and boundary plane orientation (two parameters) [9]. In the case where the misorientation parameters are ignored, the two-dimensional distribution of interface area makes it possible to calculate the “interface area aspect ratio” based on the relative areas of (0001) basal and  $(10\bar{1}0)$  prismatic facets [10]. For crystals with hexagonal symmetry, the FPA method requires  $2 \times 10^5$  boundary traces for a complete five-dimensional analysis and  $2 \times 10^3$  boundary traces to determine the two-dimensional distribution of interface area. Therefore, with a sufficient number of carbide grain boundary traces, it is possible to determine the interface area aspect ratio. Accordingly, the major purpose of the current work, which has the character of interdisciplinary composed of cemented carbide material and FPA stereological method, is to develop the method to determine the average interface area aspect ratio of carbide grains by virtue of the FPA method, and to check whether the interface

\* Corresponding author. Tel.: +86 10 67396260.

E-mail address: [yuanxiaokun@bjut.edu.cn](mailto:yuanxiaokun@bjut.edu.cn) (X. Yuan).

area aspect ratio value is sensitive to the alteration of typical processing parameters (taken densification method as an example) during WC–Co composite preparation.

## 2. Experimental

Two WC–8 wt.% Co composite samples were prepared from the WC–Co composite powder, and were obtained by different densification methods: sample 1 (similarly hereinafter) was prepared by sintering in hot isostatic press (sinter-HIP) in a 6 MPa argon atmosphere with a nominal temperature of 1500 °C maintained for 60 min, and sample 2 (similarly hereinafter) was prepared by spark plasma sintering (SPS) under an applied pressure of 50 MPa with a nominal temperature of 1200 °C maintained for 10 min. Related experimental details were introduced in a previous study [11].

The samples were prepared for electron backscattered diffraction (EBSD) analysis by polishing with a diamond abrasive and etching in Murakami's reagent (1 g potassium + 1 g sodium + 10 ml distilled water) for about 5 s, which yielded carbide surfaces suitable for EBSD mapping. The EBSD measurements were performed using a high speed Hikari camera (EDAX, Inc., USA) incorporated in a Quanta 200 scanning electron microscope (FEI Company, USA). Note that sample 1 was compressed by uniform hydrostatic pressure during Sinter-HIP, and sample 2 was consolidated by uneven pressures where the lateral pressure is often less than the axial one. To ensure the comparability between the two samples, the EBSD measurements were converged on the same direction; that is to say, the observation region for each sample is perpendicular to the axial press direction for SPS. The original EBSD data was then cleaned to correct pixels with suspicious orientations and spurious phase information.

The interface area aspect ratio is defined as the ratio of the basal surface area to the prismatic surface area and is determined by the stereological technique described in reference [8]. The observations needed for the stereological analysis are line segments that are extracted from the orientation maps and are associated with the crystal orientations. Using the FPA method, the grain boundary plane distribution (GBPD),  $\lambda(\Delta g, n)$ , is defined as the relative area of a grain boundary with a misorientation,  $\Delta g$ , and boundary plane normal,  $n$ , in units of multiples of a random distribution (MRD) [9]. When the GBPD is averaged over all misorientation,  $\lambda(n)$  presents the distribution of habit planes in the crystal frame of reference. In other words,  $\lambda(\Delta g, n)$  represents GBPD in a five-dimensional space, and  $\lambda(n)$  represents GBPD in a two-dimensional space. The current work concentrates on the two-dimensional distribution,  $\lambda(n)$  and such analysis should be accurate with 2000 line segments. Actually, sample 1 and sample 2 contained 43,078 and 54,790 line segments respectively (see details in Table 1). Therefore, the aspect ratio analysis in the current work can be regarded as reliable. Also note that in reference [10], the interface area aspect ratio is derived from the carbide/cobalt phase boundary plane distributions at the (0001) basal and (10 $\bar{1}$ 0) prismatic positions. However, in current work, most cobalt phase at the surface was removed by etching, so we merely focus on the carbide/carbide

grain boundary planes, and calculate the interface area aspect ratio from the line segments that correspond to the real carbide/carbide boundaries. In other words, the interface area aspect ratio is calculated based upon the intact carbide/carbide grain boundaries and defined as the relative area of the (0001) basal facet to the relative area of the (10 $\bar{1}$ 0) prismatic facet. Stereological programs developed at Carnegie Mellon University MRSEC are used to sort line segments according to the misorientation across the boundary and to calculate the average basal-to-prism aspect ratio described above [12].

## 3. Results and discussion

The microstructures of the two samples are illustrated by the inverse pole figure (IPF) maps in Fig. 1, where the grain color specifies the orientation according to the coloring indicated in the key. The carbide grains in both samples are differently oriented, and sample 2 has a finer grain size in comparison with sample 1, showing that grain growth is effectively inhibited during SPS process (the case for sample 2) compared with the sinter-HIP process (the case for sample 1). Note that the measured orientation texture of carbide grains in the two samples are quite different, and one possible origin might be the different pressing conditions for sintering, which might cause the dissimilar preferential orientations of carbide grains during sintering stages.

The GBPDs ( $\lambda(n)$ ) of the two samples are plotted in Fig. 2, with intensity of the distributions expressed in units of MRD. Values greater than

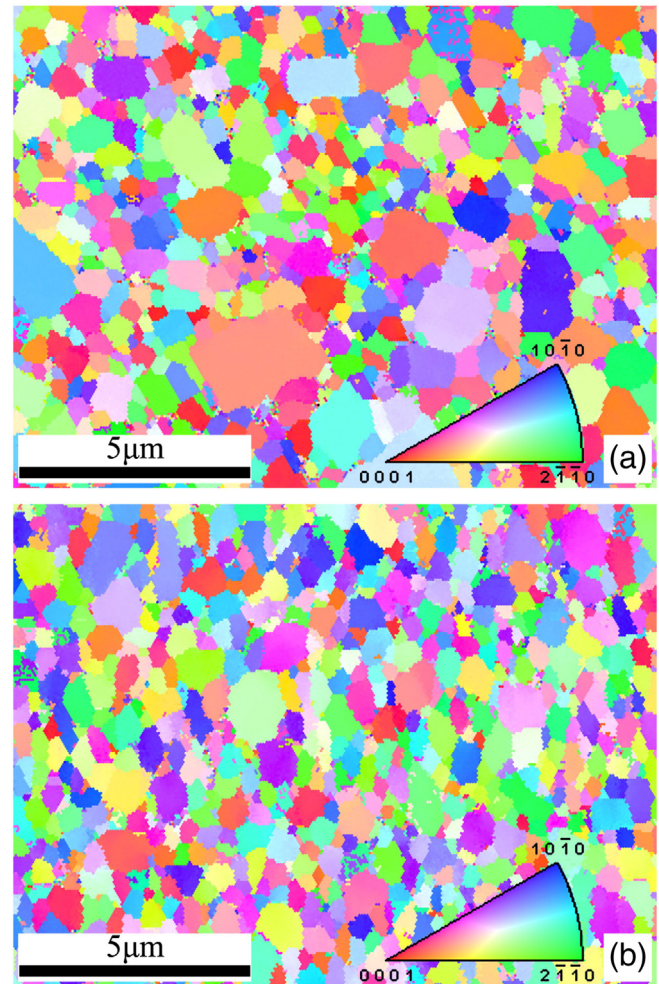
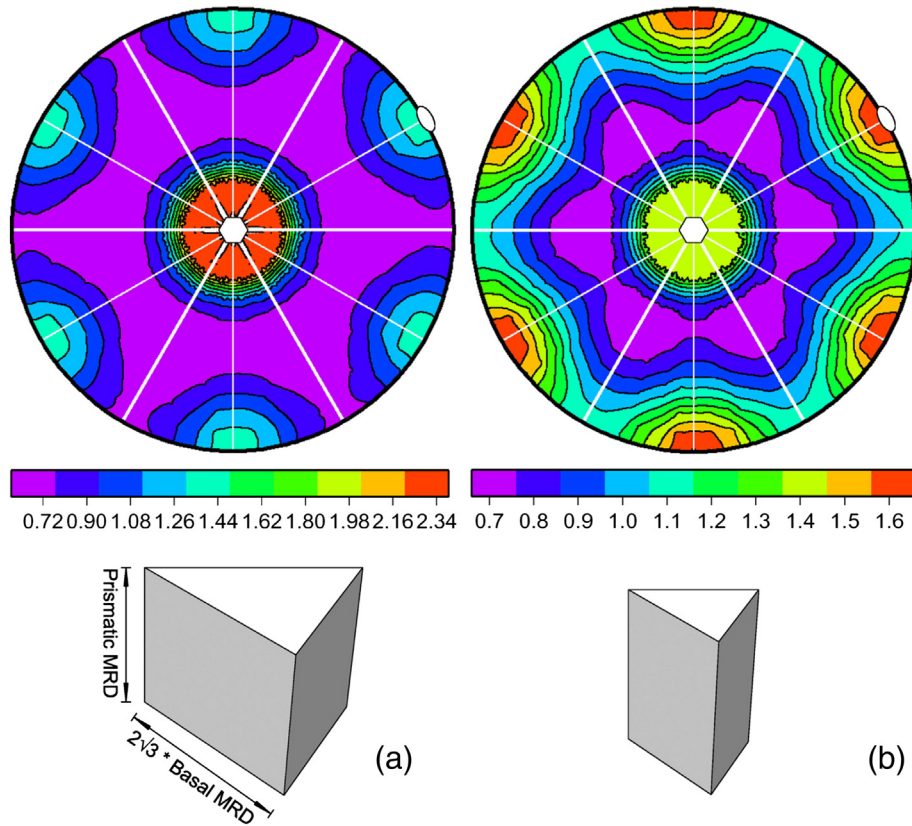


Fig. 1. Inverse pole figure (IPF) maps of the two samples, (a) sample 1, (b) sample 2, with grain orientations determined by the orientation legend for hexagonal crystallographic system. For interpretation of the color in this figure legend, the reader is referred to the web version of this article.

Table 1  
Statistics of line segments.

Statistics	Sample 1	Sample 2
Total line segment numbers	43,078	54,790
Average basal-to-prism aspect ratio	1.625	0.875
Number of line segments associated with $\Sigma 2$ boundaries	3005	5637
Average basal-to-prism aspect ratio of $\Sigma 2$ boundary planes	0.100	0.100
Number fraction of $\Sigma 2$ boundaries	6%	10%
Length fraction of $\Sigma 2$ boundaries	8.05%	13.24%
Number of line segments not associated with $\Sigma 2$ boundaries	40,073	49,153
Average basal-to-prism aspect ratio of rest boundary planes <sup>a</sup>	2.000	1.214
Number fraction of rest boundaries <sup>a</sup>	94%	90%
Length fraction of rest boundaries <sup>a</sup>	91.95%	86.76%

<sup>a</sup> "Rest boundaries" refer to the boundaries other than the  $\Sigma 2$  boundaries.



**Fig. 2.** Distribution of carbide/carbide boundary planes in sample 1 (a) and sample 2 (b). Peaks at the positions of the (0001) basal and  $(10\bar{1}0)$  prismatic planes are indicated by hexagons and ovals, with units of the contours in MRD. Idealized polygons are shown below the stereograms. For interpretation of the references to color in this figure legend, the reader is referred to the web version of this article.

one indicate the relative area associated with a specific type of plane is larger than the area that would be expected in a random distribution, and values less than one are associated with specific planes whose relative areas are less than the area that would be expected in a random distribution. For both samples, the distributions of boundary plane normals have clear preferences for the (0001) basal orientation (located at the center and marked by a hexagon) and the  $(10\bar{1}0)$  prismatic orientation (located on the periphery and marked by an oval), illustrating that the (0001) plane and  $(10\bar{1}0)$  plane are the most common habit planes.

However, the intensities at the (0001) and  $(10\bar{1}0)$  positions differ. For sample 1, habit planes with the (0001) orientation are observed 2.34 times more frequently than would be expected in a random distribution, and those with the  $(10\bar{1}0)$  orientation are observed 1.44 times more frequently than would be expected in a random distribution. For sample 2 however, the (0001) orientation and  $(10\bar{1}0)$  orientation occur 1.4 and 1.6 times as frequently as expected in a random distribution, respectively.

The results in Fig. 2 illustrate that although the samples underwent different densification procedures, the carbide crystals have consistent

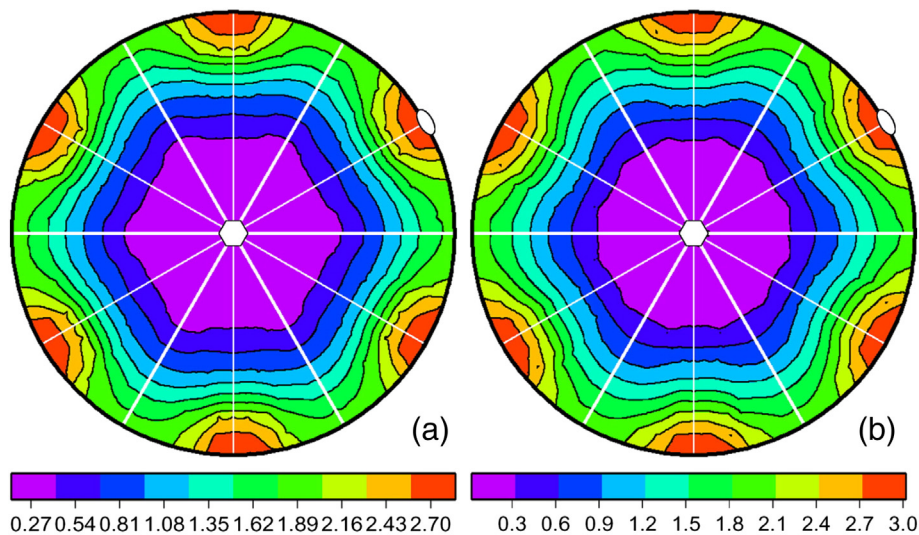


**Fig. 3.** Distribution of  $\Sigma 2$  grain boundary planes in sample 1 (a) and sample 2 (b). Peaks at the positions of the (0001) basal and  $(10\bar{1}0)$  prismatic planes are indicated by hexagons and ovals, with units of the contours in MRD. For interpretation of the references to color in this figure legend, the reader is referred to the web version of this article.

common habit planes. However, different grain sizes were obtained in the two kinds of densification processes, which can be seen in Fig. 1. In this work, idealized polygons are utilized to represent the average shape of the carbide grains, and the approach to draw such a polygon is plotting a triangular prism, the side length of the equilateral triangle basal equals to the basal MRD value multiplied by a constant of  $2\sqrt{3}$ , and the height of the triangular prism equals to the prismatic MRD value; therefore, the interface area aspect ratio equals to the ratio of the total basal area to the total prism area of the polygon; furthermore, the average grain size can be represented by the volume of the polygon. The idealized polygons are shown below the stereograms in Fig. 2, and the polygon of sample 1 is used as an example to explain the drawing geometry of polygons. For sample 1, the interface area aspect ratio is 1.625, and the idealized polygon is less equal-axied and has a larger volume, and particularly, the relatively larger basal area makes the polygon more plate-like. For sample 2, the interface area aspect ratio is 0.875, and the idealized polygon is more equal-axied; in the meantime, the polygon has a smaller volume and has a relatively larger prismatic area fraction.

On the other hand, Fig. 2 overall illustrates that the average size as well as the interface area aspect ratio of carbide grains vary with densification methods. In the current work, the sinter-HIP and the SPS were respectively taken as the representative methods of liquid-state sintering and rapid sintering technologies; therefore, differences in both average grain size and shape factor might result from the intrinsic features of the selected sintering technologies. According to an earlier study [13] focused on the microstructures that result from the sinter-HIP and SPS methods, carbide grains grow more adequately during sinter-HIP process than during the rapid SPS process. Meanwhile, a recent theory for the development of anisotropic GBPDs [14] argues that in the late stages of microstructural development, the relative areas should reach a steady state. Considering this, one can imagine that during the sinter-HIP process, the carbide grains averagely have larger size as a consequence of full development of carbide grains; on the other hand, the fully developed shape anisotropy

during this procedure makes the carbide grains less equal-axied. As a comparison, the carbide grains averagely have smaller size due to insufficient grain growth during SPS process, and the inadequate shape anisotropy development makes the carbide grains more equal-axied. The results presented in Fig. 2 are consistent with the above cognitions: as to the average grain size, if the MRD units are neglected, the idealized polygon in Fig. 2(a) has a dimensionless volume of 41, and the idealized polygon in Fig. 2(b) has a dimensionless volume of 16; as to the shape anisotropy, if the basal MRD is taken as the reference, the prismatic MRD is 38% higher than the basal MRD in sample 1, and the prismatic MRD is 14% lower than the basal MRD in sample 2. It is, therefore, concluded that the computational characterization results in Fig. 2 have their materials preparation initiations.

One of the most frequently occurring carbide/carbide boundaries has the misorientation of  $90^\circ$  about the  $[10\text{-}10]$  axis, abbreviated as the  $90^\circ/[10\text{-}10]$  boundary, or  $\Sigma 2$  boundary in coincidence site lattice (CSL) notation [15]. In a previous study [11], analysis concentrated on GBPDs ( $\lambda(\Delta g, n)$ ) for this boundary and found that the SPSed sample had more than three times the relative area of  $\Sigma 2$  boundaries compared to the sinter-HIPed sample. This means that in the SPSed sample, the total prismatic area should be larger compared to the total basal area, and this is consistent with the current findings (see Fig. 2b). Therefore, it is instructive to compare the GBPDs with  $\Sigma 2$  misorientations excluded or not.

For the two samples, line segments associated with  $\Sigma 2$  grain boundaries are sorted out, and their GBPDs ( $\lambda(n)$ ) are plotted in Fig. 3, where both samples present obvious preference for the  $(10\bar{1}0)$  planes; in other words, the  $(10\bar{1}0)$  prismatic planes occupy predominant fractions among the  $\Sigma 2$  boundary planes, which is consistent with the observed high frequency of  $\Sigma 2$  twist boundaries in previous work [11], where the  $\Sigma 2$  twist boundary that consists of  $(10\bar{1}0)$  prismatic planes on the two sides appears as the most common configuration in both sinter-HIP and SPS cases.

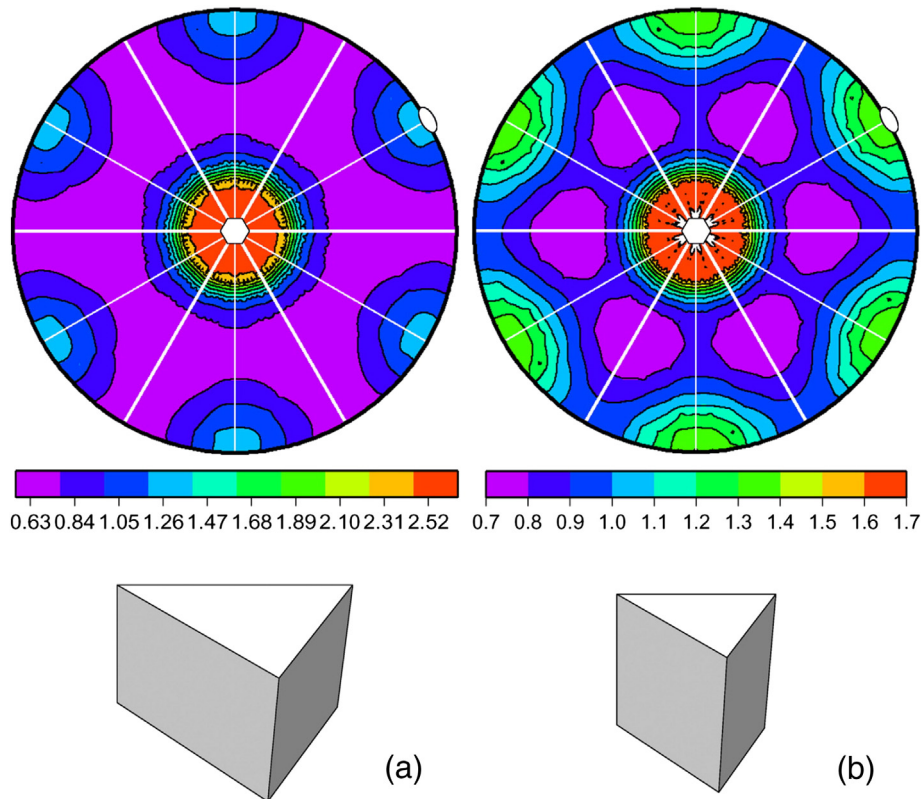


Fig. 4. Distribution of carbide/carbide boundary planes that not include  $\Sigma 2$  boundaries planes in sample 1 (a) and sample 2 (b). Peaks at the positions of the  $(0001)$  basal and  $(10\bar{1}0)$  prismatic planes are indicated by hexagons and ovals, with units of the contours in MRD. Idealized polygons are shown below the stereograms. For interpretation of the references to color in this figure legend, the reader is referred to the web version of this article.

Subsequently, the line segments for grain boundaries other than  $\Sigma 2$  were used to calculate GBPDs ( $\lambda(n)$ ), which are plotted in Fig. 4, with the idealized polygons shown below the stereograms. When the  $\Sigma 2$  boundaries and their prevalent  $(10\bar{1}0)$  prismatic planes are excluded from the boundary population, the average basal-to-prism aspect ratio associated with the rest boundaries increase in both samples. The average basal-to-prism aspect ratios turn to 2 for sample 1 and 1.214 for sample 2. As an illustration, the idealized polygons present more flat shapes due to the relative higher percentage of (0001) basal plane areas in both samples.

During sintering, the growth and shrinkage of carbide grains lead to a steady state distribution of grain sizes and shapes. The low-energy  $\Sigma 2$  boundaries are thought to play an important role during this procedure, based on the rationale that rapid grain growth is attributed to coalescence of grains along the  $\Sigma 2$  boundary planes [16]. Therefore, besides characterizing the approximative geometry of carbide grains (see the polygons in Fig. 2), the interface area aspect ratio measurement can also help to describe the grain development during sintering. For example, by comparing the polygons in Fig. 2a and b, it could be surmised that compared with sinter-HIP process, SPS process has a relatively weak grain boundary development on (0001) basal planes. In a similar way, polygon configurations corresponding to different sintering stages can be used to estimate the elimination degree of  $\Sigma 2$  twist boundaries during sintering process, and one can imagine that the grain coalescence along the  $\Sigma 2$  twist boundary planes decrease the relative area of  $(10\bar{1}0)$  prismatic planes, which in turn make the idealized polygon more plate-like. Also note that the interface area aspect ratio in this work is defined from the relative areas of carbide habit planes, and hence, such aspect ratio measurement can be applied to other tungsten carbide-based composites.

#### 4. Conclusions

Five parameter analysis method has been used to measure the interface area aspect ratios of carbide grains in WC–Co composites. Measurements of grain boundary plane distributions that averaged over all misorientations indicate that the (0001) basal and  $(10\bar{1}0)$  prismatic planes are the most common habit planes of carbide grains, and the average basal-to-prism aspect ratios are then determined by the ratio of the relative (0001) plane area to the relative  $(10\bar{1}0)$  plane area. Changes in the measured interface area aspect ratios are found to be dependent upon the densification methods. The work offers a new opportunity to describe the geometrical shapes of carbide grains in tungsten carbide-based composites.

#### Acknowledgments

GSR acknowledges support from the Office of Naval Research Grant N00014-11-1-0678. Facilities support from the Carnegie Mellon MRSEC, under National Science Foundation under Award Number DMR-0520425, is also acknowledged. XYX acknowledges supports from the National Natural Science Foundation of China 51174009. XKY acknowledges supports from the Beijing Natural Science Foundation 2123061 and the State Key Lab of Advanced Metals and Materials 2013-Z01. XKY also appreciates his colleague, Dr. Yuntao Lei, for providing kind help to this work, and thanks to Dr. Hongmei Xu for giving linguistic advice.

#### References

- [1] Rohrer GS, Saylor DM, Dasher BE, Adams BL, Rollett AD, Wynblatt P. The distribution of internal interfaces in polycrystals. *Z Metallkd* 2004;95:197–214.
- [2] Bonache V, Salvador MD, Busquets D, Burguete P, Martinez E, Sapina F, et al. Synthesis and processing of nanocrystalline tungsten carbide: towards cemented carbides with optimal mechanical properties. *Int J Refract Met Hard Mater* 2011;29:78–84.
- [3] Kim CS, Massa TR, Rohrer GS. Modeling the relationship between microstructural features and the strength of WC–Co composites. *Int J Refract Met Hard Mater* 2006;24:89–100.
- [4] Shatov AV, Firstov SA, Shatova IV. The shape of WC crystals in cemented carbides. *Mater Sci Eng A* 1998;242:7–14.
- [5] Liu T, Raabe D. Influence of nitrogen doping on growth rate and texture evolution of chemical vapor deposition diamond films. *Appl Phys Lett* 2009;94:021119.
- [6] Zhong Y, Zhu H, Shaw LL, Ramprasad R. The equilibrium morphology of WC particles – a combined ab initio and experimental study. *Acta Mater* 2011;59:3748–57.
- [7] Shaw LL, Luo H, Zhong Y. WC-18 wt.% Co with simultaneous improvements in hardness and toughness derived from nanocrystalline powder. *Mater Sci Eng A* 2012;537:39–48.
- [8] Saylor DM, Rohrer GS. Determining crystal habits from observations of planar sections. *J Am Ceram Soc* 2002;85:2799–804.
- [9] Saylor DM, Dasher BS, Adams BL, Rohrer GS. Measuring the five-parameter grain boundary distribution from observations of planar sections. *Metall Mater Trans A* 2004;35:1981–9.
- [10] Kim CS, Massa TR, Rohrer GS. Interface character distributions in WC–Co composites. *J Am Ceram Soc* 2008;91:996–1001.
- [11] Yuan XK, Song XY, Chien H, Li J, Rohrer GS. Effect of densification mechanism on the  $\Sigma 2$  grain boundary plane distribution in WC–Co composites. *Mater Lett* 2013;92:86–9.
- [12] <http://mimp.materials.cmu.edu/~gr20/stereology> (accessed March 7, 2013).
- [13] Wei CB, Song XY, Fu J, Liu XM, Gao Y, Wang HB, et al. Microstructure and properties of ultrafine cemented carbides – differences in spark plasma sintering and sinter-HIP. *Mater Sci Eng A* 2012;552:427–33.
- [14] Dillon SJ, Rohrer GS. Mechanism for the development of anisotropic grain boundary character distributions during normal grain growth. *Acta Mater* 2009;57:1–7.
- [15] Hagege S, Nouet G, Delavignette P. Grain boundary analysis in TEM (IV) coincidence and the associated defect structure in tungsten carbide. *Phys Status Solidi A* 1980;62:97–107.
- [16] Kumar V, Fang ZZ, Wright SI. An analysis of grain boundaries and grain growth in cemented tungsten carbide using orientation imaging microscopy. *Metall Mater Trans A* 2006;37:599–607.